A Bayesian and Minimum Variance Technique for Arterial Lumen Segmentation in Ultrasound Imaging

Sergio Rogelio Tinoco-Martínez, Felix Calderon, Carlos Lara-Alvarez, and Jaime Carranza-Madrigal

División de Estudios de Posgrado, Facultad de Ingeniería Eléctrica, Universidad Michoacana de San Nicolás de Hidalgo, Santiago Tapia 403, Centro, 58000 Morelia, Michoacán, México
http://www.umich.mx/

Abstract. Cardiovascular diseases (CVDs) are the worldwide leading cause of deaths. Based on ultrasound, primary assessment of CVDs is measurement of carotid intima-media thickness and brachial endothelial function. In this work we propose improvements to a state of the art automatic methodology for arterial lumen detection, based on graphs and edge detection, fundamental for cited tests. We propose a bayesian approach for segmenting the graph minimum spanning tree created with points between edges. Lumen is located applying three criteria on segmented trajectories: length, darkness, and our proposal, minimum variance. In 294 sonograms having manually established measurements, from a 1,104–sonogram set, mean and standard deviation error in brachial near wall detection was 14.6 μm and 17.0 μm, respectively. For far wall they were 15.1 μm and 14.5 μm, respectively. Our methodology maintains superior performance to results in recent literature that the original methodology presents, but surpasses it in overall accuracy.

Keywords: automatic detection, ultrasonography, carotid, brachial, lumen, bayesian, variance, graphs, polynomial fitting.

1 Introduction

Cardiovascular diseases (CVDs) are the worldwide leading cause of deaths [26]. The most disturbing pathology associated with CVDs is atherosclerosis, a progressive degeneration that reduces the *arterial lumen* (AL) and causes arterial wall thickening. Progressive development of this disease has been correlated with increased risk of CVDs [16].

Based on ultrasound, primary markers for CVDs and atherosclerosis assessment are measurement of the carotid intima-media thickness (IMT) [1], and measurement of the brachial artery endothelial function (BAEF) [4].

The IMT and BAEF tests require the detection of carotid and brachial lumen, respectively, in order to run properly. Calderon et al. [2] proposed in 2013 a graph-based algorithm for automatic AL detection in *ultrasound images* (USIs).

F. Castro, A. Gelbukh, and M. González (Eds.): MICAI 2013, Part I, LNAI 8265, pp. 545–557, 2013.

The algorithm first determines edges of the *ultrasound image* (USI), and then creates a graph with intermediate points between consecutive detected edge points (in a column basis). Later, it calculates the graph *minimum spanning tree* (MST), and does a segmentation process of those trajectories likely to be the true AL, using only a criterion based on distance between connected nodes.

Trajectory representing the true AL is selected from those segmented ones, based on a linear combination of a length and a darkness criteria.

Calderon et al. pointed out that their algorithm has superior performance to results reported in recent literature in this area. Nevertheless, in this paper we propose solution to two deficiencies their algorithm has.

Remainder of this paper is organized as follows: Section 2 presents a brief review of recent work in the area; Section 3, poses problems whose solution we propose in this article; Section 4, details the bayesian hypothesis test used for validating the trajectories segmentation process referred to in Section 3; Section 5 describes the *minimum variance criterion* (MVC) that is used to discriminate the true AL in those cases where the length criterion presents the inconsistencies explained in Section 3; Section 6, summarizes the methodology presented in this research for automatic AL detection in USIs; Section 7, describes tests performed and results obtained when methodology presented in Section 6 is applied on an USI set; and, Section 8, summarizes conclusions reached with work carried out.

2 Previous Work

In the absence of atherosclerotic plaque, B–mode ultrasound shows the wall of an artery as a regular pattern that correlates with anatomical layers. In the USI, the AL may be observed as a dark region flanked on its top and bottom by bright light stripes, which will turn out as edges considering the intensity profile of the pixels. Under this assumption, works presented in literature for arterial vessel segmentation apply different methods to locate these contrasting zones, and thus, determining both the lumen and different arterial measurements.

Early work is based on edge detection [17,22] and, later, on image gradient [12,20,8]. Methods included in these categories are fast in their calculation but sensitive to noise, artery morphology, and require manual intervention to get good results.

Other approaches apply linear programming [18,23] in order to establish a cost function based on a linear combination of several weighted measurements calculated from the USI, to segment the artery and the layers that it is made of. It has also been proposed [11] to apply this method at different USI scales to reduce computational cost. Techniques in this category can be fully automated, which limits variability in final results [24,9] due to skills and operator fatigue. However, they require system training and are sensitive to image noise, which directly affects the cost function.

The most used technique for arterial segmentation is the active parametric contours [25] or *snakes*, which adapts a deformable linear model to the border between the AL and the intima layer. Most of the published works [13,16,5]

adopt the snakes formulation presented in [25]. Application of this method has not been fully automated; besides, is very sensitive to noise, requires tuning of those parameters that define the snakes, and results depend on chosen starting points as well as their number.

Other proposals consists in calculating local statistics on intensity of the USI pixels, coupled with the establishment of an acceptance/rejection threshold on membership of these pixels to the AL area [5]. It has also been proposed to improve this technique [14,6] using a fuzzy k-means classifier as an initialization stage for a snakes-based method to refine the detection process.

Hough transform has also been proposed for the arterial segmentation [10,21]. In longitudinal USIs the goal is to delineate dominant lines of the boundary between lumen and arterial walls, and in transversal USIs, the goal is to delineate the same boundary, but outlined as a circumference. Although Hough transform calculation is fast, it is effective only when processing images in which the artery appears in a straight and horizontal way.

Finally, a recent work has proposed a fully automated technique for arterial detection [16] based on local maxima in pixels intensity of the USI, applying a linear discriminant to these *seed points*, with a fuzzy k-means classifier as a refinement stage.

Next section outlines deficiencies of the methodology proposed by Calderon et al. for AL detection in USIs, and whose solution we propose in this article.

3 Problem Statement

Work presented by Calderon et al. in [2] faces difficulties in recognizing an AL in an USI that has noticeable discontinuities or cuts at the edges. To illustrate this, Fig. 1(a) shows trajectories likely to be selected as the true AL in a test USI, applying this algorithm.

When the graph MST is segmented, based on distance-between-connected-nodes criterion, trajectory that belongs to the true AL is broken into several ones (2 and 3 in Fig. 1(a)). In consequence, trajectory 1 is mistakenly chosen as the true AL. The solution proposed for this problem is to validate segmentation process by the hypothesis testing detailed in Section 4.

Equally important, when length criterion value l_i for two or more trajectories that represent options likely to be selected as the real AL are above a certain threshold u_{cl}, algorithm of Calderon et al. is unable to select the correct choice.

To illustrate this, we take the USI in Figure 1(b) as an example. Trajectory 0 in this figure has 0.98661, 0.95766, and 1.94427 as values for the length, darkness, and their linear combination criteria, respectively. Trajectory 4 has 1.0, 0.87787, and 1.87787 as values for the same criteria. If we select the true AL based on length criterion, trajectory 4 would be correctly selected as the AL. If we select the true AL based on darkness criterion, trajectory 0 would be incorrectly selected as the AL. Finally, selection of Calderon et al. is based on the maximum linear combination of both criteria, i.e., trajectory 0 is selected as the AL, which is incorrect for this specific USI. To solve the problem above, without affecting overall performance of methodology, the MVC, explained in Section 5, is proposed.

Calderon et al. indicate that, for the whole set of test USIs, combination of length and darkness criteria produces the best results to select the real AL.

The following section describes in detail the procedure for validating the segmentation process that is used as part of the methodology for automatic AL detection presented in this paper.

4 Hypothesis Testing

To reduce over-segmentation produced by the methodology of Calderon et al., we propose to validate this segmentation process using a hypothesis testing [19].

Given point sets $D_1 = \{p_i\},\ p_i = [x_i, y_i]^T$ and $D_2 = \{p_j\},\ p_j = [x_j, y_j]^T$; such that $D_1 \cap D_2 = \emptyset$, of size N_1 and N_2, respectively; which have associated corresponding polynomial approximations $f(x_i; a_1)$ and $f(x_j; a_2)$ given by:

$$f(x; a) = a_0 + a_1 x + a_2 x^2 + a_3 x^3 + \cdots + a_m x^m \ . \tag{1}$$

One of the following hypotheses has to be demonstrated:

H_0**:** Sets D_1 and D_2 are partitions of the same set D ($D = D_1 \cup D_2$), therefore, they can be characterized by a unique polynomial approximation $f(x, a)$.

H_1**:** Sets D_1 and D_2 are not partitions of the same set, therefore, they are characterized by polynomial approximations $f(x_1, a_1)$ and $f(x_2, a_2)$, respectively.

Decision criterion will be probabilistic, so that hypothesis H_0 will be valid if and only if (2) holds. Otherwise, the fulfilled hypothesis will be H_1.

$$P(H_0 \mid D_1, D_2) > P(H_1 \mid D_1, D_2) \ . \tag{2}$$

Applying Bayes' theorem and assuming that probability of both hypotheses is the same, $P(H_0) = P(H_1)$, the final decision criterion can be expressed as (3).

$$P(D_1, D_2 \mid H_0) > P(D_1, D_2 \mid H_1) \ . \tag{3}$$

In order to use decision criterion (3), probabilities $P(D_1, D_2 \mid H_0)$ and $P(D_1, D_2 \mid H_1)$ need to be estimated. We begin by estimating $P(D \mid H_0)$, given that D is a single data set; for this, we assume that any polynomial with parameters a has the same probability of being selected, therefore, it follows a uniform distribution, $P(a \mid H_0) = k_1$; and that errors between approximation $f(x_i, a)$ and the actual measurements y_i, follow a Gaussian model given by (4).

$$P(D \mid a, H_0) = k_1 \exp\left(-\frac{E(a)}{2\sigma^2}\right) = k_1 \exp\left(-\frac{\sum_{i=1}^{N} \left(f(x_i; a) - y_i\right)^2}{2\sigma^2}\right) \ . \tag{4}$$

Then, $P(D \mid H_0)$ can be written, considering the total probability law, as:

$$P(D \mid H_0) = k_1 k_2 \int_{\Omega} \exp\left(-\frac{E(a)}{2\sigma^2}\right) d^m a \ . \tag{5}$$

where Ω is the function domain, which is integrated in m dimensions.

In order to solve (5), we determine the Taylor series expansion at point a^*, which is the least squares solution for $E(a)$, and integrate the exponential function in m dimensions [19], which give us:

$$P(D \mid H_0) = k_1 k_2 \sqrt{\frac{(4\pi\sigma^2)^m}{|\nabla^2 E(a^*)|}} \exp\left(-\frac{E(a^*)}{2\sigma^2}\right) . \tag{6}$$

For calculation of probability $P(D_1, D_2 \mid H_1)$, assume that data sets D_1 and D_2 were generated by independent models, so that it can be written as:

$$P(D_1, D_2 \mid H_1) = P(D_1 \mid H_0) P(D_2 \mid H_0) . \tag{7}$$

Probabilities $P(D_1 \mid H_0)$ and $P(D_2 \mid H_0)$ are calculated using (6), and the obtained result for (7) is given by (8):

$$P(D_1, D_2 \mid H_1) = \frac{k_1^2 k_2^2 (4\pi\sigma^2)^m}{\sqrt{|\nabla^2 E(a_1^*)||\nabla^2 E(a_2^*)|}} \exp\left(-\frac{E(a_1^*) + E(a_2^*)}{2\sigma^2}\right) . \tag{8}$$

Sets D_1 and D_2 will be join if $P(D \mid H_0) > P(D_1, D_2 \mid H_1)$.

Next section describes the MVC, referred to in Section 3, for selecting the AL in those cases where the length criterion is inconsistent.

5 Minimum Variance Criterion

For AL selection cases where length criterion value exceeds a threshold u_{cl} for two or more trajectories, we propose to use a MVC as a third discrimination criterion for selecting the true AL.

According to a radiologist observations and criteria, it can be considered that an AL has a smooth curvature in an USI, thus, when image edges are detected, the number of outlier edge points will be fewer as compared to the number in detected edges of channels or anatomical structures that resemble it. One way to calculate this is using the sample variance of the edge points.

We will do the variance calculation over the elements of a set S_{u}, comprised of the trajectories set whose number of edge points is greater than 95% of the number of points corresponding to the anatomical structure in the USI with the greatest number of them.

For our noise model given by (4), sample variance for the j-th anatomical structure in the USI can be calculated as:

$$\sigma_j^2 = \frac{1}{N_j - 1} \sum_{i=1}^{N_j} \left(f(x_i; a_j^*) - y_i\right)^2 . \tag{9}$$

MVC points out that the true AL is the one trajectory, given by (10), having the minimum value of the sample variance:

$$\min_j j^* = \sigma_j^2, \ j \in \{1, 2, \ldots, |S_{\mathrm{u}}|\} . \tag{10}$$

Note that the MVC is used only in those cases where more than one trajectory exists, i.e., that $|S_u| > 1$. Otherwise, linear combination of length and darkness criteria is used, as proposed by Calderon et al.

For USI in Fig. 1(b), we have that trajectories 0 and 4 have similar values of length criterion, but sample variance calculated with (9) gives us $\sigma_0 = 2.2321$ and $\sigma_4 = 0.3649$. It follows from the aforementioned that the selected true AL is given by trajectory 4.

Figure 1(c) shows the USI in Fig. 1(b), with the superimposing of the edges of the detected AL, based on the MVC.

The following section describes the methodology of Calderon et al. with changes we propose, for the AL segmentation in USIs.

6 Methodology

Detection procedure begins with an automatic histogram-based clipping of the USI, which removes information not necessary for the AL segmentation process. Resulting image is referred to as the original image I.

An USI I is defined as a set of pixels $I(p_i)$, which represents a gray tone in a point having coordinates $p_i = [x_i, y_i]^T$, over image grid R of size $N_{\text{Cols}} \times N_{\text{Rows}}$.

Next, and under the assumption that the AL in an USI is presented as a dark region flanked on its top and bottom by much clearer areas, edges of image I are detected using Canny's algorithm [3]. These detected edges are represented as a set B, containing N_B coordinate points $b_i = [x_i, y_i]^T$ such that:

$$B = \{b_i \in R \mid g(b_i) = 1, \forall b_i \in R\} \tag{11}$$

where g is a binary image of same size as I, defined in (12).

$$g(b_i) \equiv g(x_i, y_i) = \begin{cases} 1 & \text{if } b_i \text{ is an edge,} \\ 0 & \text{otherwise.} \end{cases} \tag{12}$$

Later, a column c of image g, a vector of 0s and 1s like (13), is built.

$$g(c, \ldots) = [0, 0, 1, 0, 1, 0, 0, 0, 1, 0, 0, 0, 1, 0, 0, 1, 0, 0 \ldots]^T \,. \tag{13}$$

Representation of these edges is done by storing their coordinates in an ordered array. For edge column in (13), its representation is given by (14):

$$\hat{B}_c = \{[c, 3]^T, [c, 5]^T, [c, 9]^T, [c, 13]^T, [c, 16]^T, \ldots\} = \{\hat{b}_k, \hat{b}_{k+1}, \hat{b}_{k+2}, \ldots\} \tag{14}$$

and the ordered representation of all edges of image I, equivalent to (11), is (15):

$$\hat{B} = \{\hat{B}_1, \hat{B}_2, \ldots, \hat{B}_c \ldots, \hat{B}_{N_{\text{Cols}}}\} = \{\hat{b}_1, \hat{b}_2, \hat{b}_3, \ldots, \hat{b}_k, \hat{b}_{k+1}, \hat{b}_{k+2} \ldots\} \,. \tag{15}$$

With this, there will be a couple of points $< \hat{b}_i, \hat{b}_{i+1} >$ in each column of the image with all edges, candidates to be the AL limits.

Methodology continues discarding pairs of consecutive edge points whose separation distances are below a preset threshold A_{Min}. Thus, set of points B_{L} is defined, based on the ordered set of points $\hat{B} \equiv B$, as follows:

$$B_{\text{L}} = \{\hat{b}_1, \hat{b}_2, \ldots, \hat{b}_i, \hat{b}_{i+1} \ldots \mid (\hat{y}_{i+1} - \hat{y}_i) \geq A_{\text{Min}},\ \hat{x}_i = \hat{x}_{i+1}\} \,. \tag{16}$$

B_{L} set is a subset of edge set B, therefore, lumen search universe is reduced.

It is also defined V, the set of points half of the way between the likely lumen limits given by the set B_{L}, as:

$$V = \{v_i \mid v_i = \frac{\hat{b}_i + \hat{b}_{i+1}}{2},\ \hat{x}_i = \hat{x}_{i+1}, \forall \hat{b}_i \in B_{\text{L}}\} \,. \tag{17}$$

In this way, for a point v_i exists an associated pair $< \hat{b}_i, \hat{b}_{i+1} >$ such that $\hat{b}_i < v_i < \hat{b}_{i+1}$, and the three of them are in the same column of image g.

Figure 1(d) shows points of sets B_{L} and V, superimposed on image I. Points of set V are the options likely to be selected as the center of the real lumen.

Subsequently, an undirected graph $G = \{V, A\}$ is built from point set V, defined in (17). V represents the graph nodes set, and A the set of graph edges. Initially all nodes are connected, and the weight of each graph edge, A_{ij}, is the Euclidean distance $d(v_i, v_j)$ between points of set V the edge connects.

Afterwards, the undirected graph is segmented and classified using weights $d(v_i, v_j)$, supporting these cutting process by the bayesian hypothesis test from Section 4. The minimum spanning tree (MST) G^+ for graph G, is calculated using Kruskal's algorithm. Figure 1(g) shows an example of created G^+.

In order to take the true AL trajectory out from the graph, a set S of N_{G} subgraphs is defined in (18). This set is the result of segmenting G^+, when cutting graph edges whose distances $d(v_i, v_j) > p_{\text{Max}}$ (a cutoff threshold), and that meet hypothesis H_1 (from Section 4) for nodes corresponding to subgraphs G_i^+ and G_j^+ that are connected by graph edge A_{ij}. Otherwise, when fulfilled hypothesis is H_0, graph edge A_{ij} is kept intact, even when distance $d(v_i, v_j)$ exceeds p_{Max}. Cuts are carried out using a depth-first traversal on G^+.

$$S = \{G_1^+, G_2^+, \ldots, G_{N_{\text{G}}}^+\} \,. \tag{18}$$

Figure 1(g) shows the graph MST, created with points indicating options likely to be selected as the center of the true AL for a test USI. Double-headed arrow marked as H_1 is an example of graph edge that exceeds distance threshold p_{Max}, and that meets hypothesis H_1; so to be cut. Single-headed arrow H_0 is an example of a graph edge that exceeds distance threshold p_{Max}, but that meets hypothesis H_0; so that should remain intact.

Process continues removing short trajectories that exist due to noise or muscle tissue layers in the USI. Hence, subgraphs G_i^+ which have a total node number below a threshold N_{Min} are eliminated from set S, defining subgraph set S^+ as:

$$S^+ = S - \{G_i^+ \in S \mid N_{S_i} < N_{\text{Min}}\}, \quad i \in \{1, 2, \ldots, N_{\text{G}}\} \tag{19}$$

being N_{S_i} the node number of subgraph G_i^+.

Options likely to be the true AL has been decreased considerably up to this point, but there are still more than one option, so that the real AL is selected using the length, minimum variance, and darkness criteria.

Length criterion calculates total node number on each subgraph $G_i^+ \in S^+$, normalized between [0, 1], according to the following equation:

$$l_i = \frac{N_{S_i}}{\max(N_{S_1}, N_{S_2}, \ldots, N_{S_{|S^+|}})}, \quad i \in \{1, 2, \ldots, |S^+|\} \; . \tag{20}$$

Now, if at the time of calculating length criterion l_i for each subgraph G_i^+, it happens that more than one $l_i > u_{\text{cl}}$, the MVC (Section 5) will be used to determine the correct AL of the USI. Otherwise, the AL selection will be based on a linear combination of both length and darkness criteria.

For the darkness criterion the average value μ_j of gray tones of the correspondig area for each subgraph $G_j^+ \in S^+$is calculated. To this end, each subgraph is traversed in each of its points v_i, sweeping in a column basis at intervals $[\hat{b}_i, \hat{b}_{i+1}]$ (according to (17)) of the original image I, as formulated next:

$$\mu_j = \frac{1}{N_{S_j^+}} \sum_{\forall v_i \in G_j^+} \left[\frac{1}{\hat{y}_{i+1} - \hat{y}_i + 1} \sum_{\forall p \in [\hat{b}_i, \hat{b}_{i+1}]} I(p) \right], \quad \forall j \in \{1, 2, \ldots, |S^+|\} \tag{21}$$

being $N_{S_j^+}$ the node number in subgraph S_j^+.

Once the average is calculated, the darkness criterion is:

$$o_i = 1 - \frac{\mu_i}{\max(\mu_1, \mu_2, \ldots, \mu_{|S^+|})}, \quad \forall i \in \{1, 2, \ldots, |S^+|\} \; . \tag{22}$$

Darkness criterion, just as the length one, is normalized to range [0, 1] so they can be combined. That is, the subgraph corresponding to the center of the true AL is the one with the maximum value of the sum of both criteria:

$$\max_i i^* = (l_i + o_i), \quad \forall i \in \{1, 2, \ldots, |S^+|\} \; . \tag{23}$$

Figures 1(e) and 1(h) show two examples of arterial USIs with superimposed edges corresponding to detected lumen in each case. In Fig. 1(e), corresponding to Fig. 1(a), an example of detection based on length and darkness criteria is shown. In Fig. 1(h), corresponding to Fig. 1(b), an example of detection based on MVC is shown.

Last step of proposed technique for AL detection fits a polynomial $f(x, a)$ of degree m, by means of the least squares method, to each of the point sets belonging to the edges of the detected AL. That is, to the sets of edge points $<\hat{b}_{i^*}, \hat{b}_{i^*+1}>$, related to the points $v_{i^*} \in G_{i^*}^+$.

Polynomial fitting is performed to the set of edge points $\hat{b}_{i^*}$ first, belonging to the edge $f_{\text{N}}(\hat{x})$ between the lumen and the near wall of the artery; and, later, to the set of edge points $\hat{b}_{i+1}^*$, belonging to the edge $f_{\text{F}}(\hat{x})$ between the lumen and the far wall of the artery.

In order to strengthen the polynomial fitting against noise in the USI, estimation of the polynomial model parameters is directed by means of the *RANdom SAmple Consensus* (RANSAC) algorithm.

Figure 1(f) shows the image with the fitted polynomial approximations by the least squares method and the RANSAC algorithm, on points of the AL edges shown in Fig. 1(e). Robust polynomial approximations, corresponding to Fig. 1(h), are shown in Fig. 1(c).

Once described the proposed AL detection methodology, the section below details tests and results obtained from its application.

7 Tests and Results

Tests were carried out on same database of USIs provided to Calderon et al. by the laboratory *Centro Unión* of Morelia, Michoacán, México. This database consists of 1,104 longitudinal B–mode ultrasound two-dimensional images of carotid and brachial arteries. All images were transferred to the computer through a DICOM communication port and logarithmically compressed to an 8-bit grayscale (256 gray shades). Axial resolution of the USIs is 76.9 μm per pixel.

Parameters of the methodology were adjusted as follows: $A_{\text{Min}} = 20$ pixels, $p_{\text{Max}} = 10$ pixels, $N_{\text{Min}} = 100$ nodes, fitting polymonials degree $m = 3$, $\sigma = 32.0$ for bayesian hypothesis testing, and threshold $u_{\text{cl}} = 0.95$.

Initial test was to apply our methodology on each of the 1,104 USIs in the database then verify, qualitatively, the percentage of them in which correct pattern of a dark area flanked up and down by clearer areas was selected. In this test, 51 failures in the 1,104 USIs were found. Meanwhile, the algorithm of Calderon et al. failed in 85 of the same 1,104-USI set. This is, with proposed solutions to problems detailed in Section 3, our method accurately detected the AL in 34 pictures more than the original algorithm.

Later tests were carried out on the 294 USIs from general set which have measurements manually established by a radiologist. Process consisted in applying our technique to each image to get polynomial aproximations $f_{\text{N}}(\hat{x})$ and $f_{\text{F}}(\hat{x})$, for near and far arterial walls, respectively. Finally, error between manually established points $[x_{\text{N}}, y_{\text{N}}]^T$, $[x_{\text{F}}, y_{\text{F}}]^T$; and the estimated ones $f_{\text{N}}(x_{\text{N}})$, $f_{\text{F}}(x_{\text{F}})$; were calculated. Results for these tests are presented in Table 1.

Table 1. Error in measurements of the lumen-intima interface

	Near Wall	Far Wall
Average	14.6 μm (1.8 pixels)	15.1 μm (1.9 pixels)
Standard Deviation	17.0 μm (2.2 pixels)	14.5 μm (1.9 pixels)

Calderon et al. pointed out that based on results reported in recent literature on the AL detection area, the automatic technique that achieves best performance [15] has an average error on the far wall of 35.0 μm $\pm$ 32.0 μm. Besides,

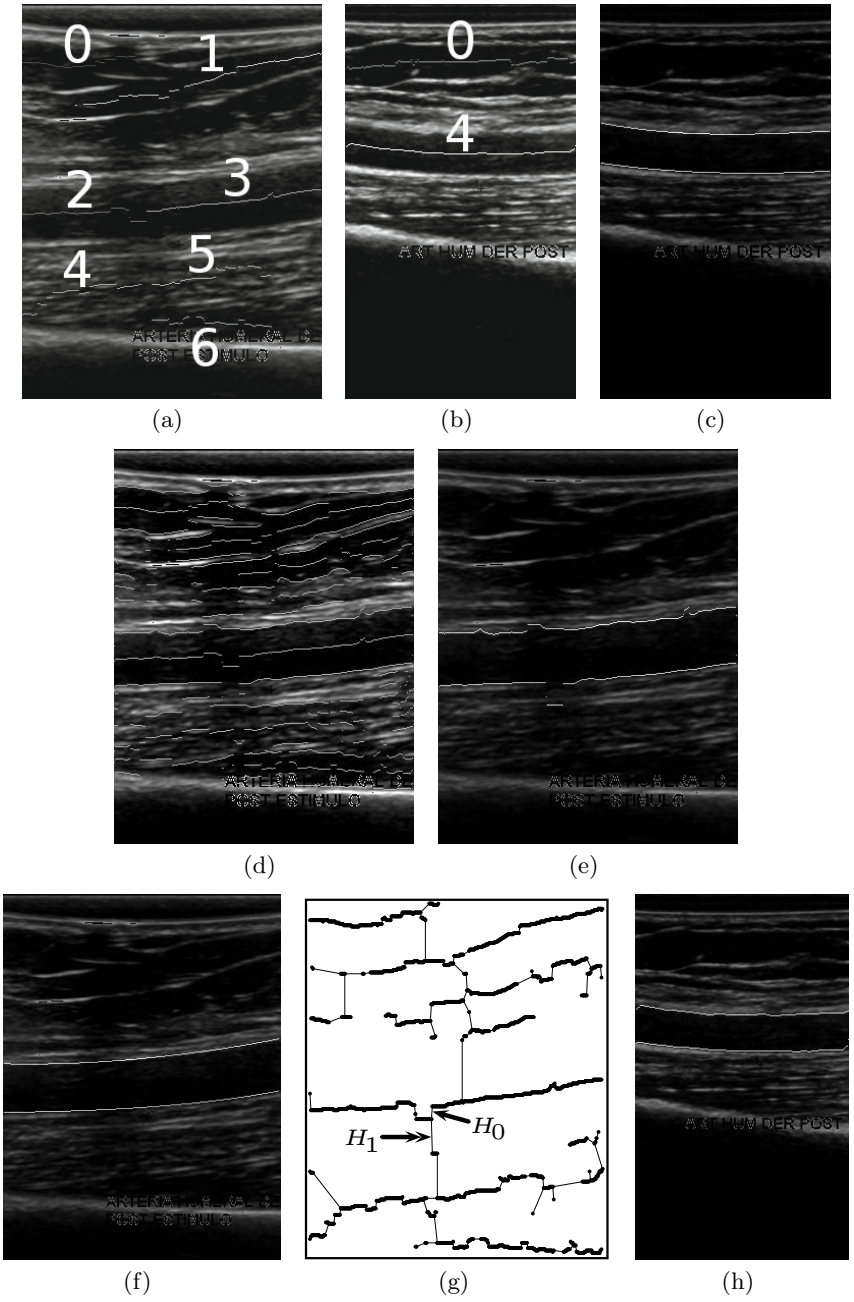

Fig. 1. (a) Options likely to be selected as the AL. (b) Inconsistency example. (c) Edges detected based on MVC (with polynomial fitting). (d) Points belonging to sets B_{L} and V. (e) Edges detected based on length and darkness criteria. (f) Polynomial fitting. (g) MST. (h) Edges detected based on MVC.

the semiautomatic technique best performed [7] has an average error on the same wall of $21.0\,\mu$m $\pm$ $13.0\,\mu$m. In relation to the arterial near wall, they pointed out that only in work presented in [14] the obtained average error is given, which is of $75.0\,\mu$m $\pm$ $56.3\,\mu$m.

Based on results shown in Table 1, methodology presented in this paper maintains superiority of proposed technique by Calderon et al. over reported performance in recent studies for automatic [15] and semi-automatic [7] detection of the arterial far wall, as well as detection of the arterial near wall [14]. Moreover, our methodology produces an average improvement of $0.3\,\mu$m in locating of the arterial far wall, over results of Calderon et al. On the other hand, in the near wall, our approach produces an average reduction of $0.7\,\mu$m. However, this result is generated at the expense of correctly detecting the AL in 34 USIs beyond those from the original methodology. Besides, additional number of images consists of USIs with features that generate greater difficulty in the discrimination process of the AL; which is markedly accounted for in results reported for our algorithm, and detection failures for the algorithm of Calderon et al.

It is worth mentioning that the algorithmic complexity of the hypothesis testing in (6) and (8) comes from the least squares solutions, which are of $\mathcal{O}(m^2(N_1+N_2))$. Calculation of Hessian determinants in (6) and (8) are of $\mathcal{O}(m^3)$ but, given that in our tests $m = 3$, we consider only the former. Also, calculating the MVC in (9) is of $\mathcal{O}(m^2 N_j)$, coming from the least squares fitting, as well. Meanwhile, the stages of the methodology with bigger complexity order, the edge detection and the MST calculation, have corresponding $\mathcal{O}(k_{\mathrm{s}}^2 N_{\mathrm{Cols}} N_{\mathrm{Rows}})$ (being k_{s}^2 the size of the convolutional kernel) and $\mathcal{O}(N^2 \log(N))$, respectively.

Considering the above and that the edge detector is applied to the whole USI, that the MST is calculated from all the USI borders, and that the hypothesis testing and the MVC are calculated for only a few trajectories, it follows that the complexity we added to the methodology of Calderon et al. is not significant because $\mathcal{O}(k_{\mathrm{s}}^2 N_{\mathrm{Cols}} N_{\mathrm{Rows}}) > \mathcal{O}(N^2 \log(N)) >> \mathcal{O}(m^2(N_1 + N_2)) + \mathcal{O}(m^2 N_j)$ due to $N_{\mathrm{Cols}} N_{\mathrm{Rows}} >> N_1, N_2, N_j$.

8 Conclusions

We presented a technique for automatic arterial lumen detection in carotid and brachial ultrasound images, which proposes a bayesian and a minimum variance criteria to address some flaws in methodology by Calderon et al. in [2].

Methodology in this work, as well as the original one, is robust to arterial morphology and orientation in an ultrasound image but, unlike the original, is robust with relation to discontinuities or cuts in the arterial edges. However, it is vulnerable to arterial pathologies or abnormal echogenic characteristics.

It should be noted that both our proposal and the original one, find the limit of their application in the edge detection algorithm. If this algorithm is unable to detect the arterial edges, for instance due to noise, the arterial lumen detection methodology will also be unable to select the correct arterial lumen.

Finally, in a laptop with an Intel® Core™ i5 at 2.30GHz processor, 4GB of memory, and software developed (but not yet speed-optimized) with the Open

Java Development Kit 7, on a Debian GNU/Linux system with a 64-bit kernel version 3.2.0, our technique processes each ultrasound image in a variable time up to 30 seconds. Nevertheless, we believe that real-time execution is possible, by means of process optimization and parallel processing use.

References

1. Amato, M., Montorsi, P., Ravani, A., Oldani, E., Galli, S., Ravagnani, P.M., Tremoli, E., Baldassarre, D.: Carotid intima-media thickness by B-mode ultrasound as surrogate of coronary atherosclerosis: Correlation with quantitative coronary angiography and coronary intravascular ultrasound findings. European Heart Journal 28(17), 2094–2101 (2007)
2. Calderon, F., Tinoco-Martínez, S.R., Carranza-Madrigal, J.: Un algoritmo basado en grafos para la detección automática de la luz arterial en imágenes ultrasonográficas. Revista Iberoamericana de Automática e Informática Industrial (to appear, 2013)
3. Canny, J.: A computational approach to edge detection. IEEE Transactions on Pattern Analysis and Machine Intelligence PAMI-8(6), 679–698 (1986)
4. Celermajer, D.S., Sorensen, K.E., Bull, C., Robinson, J., Deanfield, J.E.: Endothelium-dependent dilation in the systemic arteries of asymptomatic subjects relates to coronary risk factors and their interaction. Journal of the American College of Cardiology 24(6), 1468–1474 (1994)
5. Delsanto, S., Molinari, F., Giustetto, P., Liboni, W., Badalamenti, S., Suri, J.S.: Characterization of a completely user-independent algorithm for carotid artery segmentation in 2-D ultrasound images. IEEE Transactions on Instrumentation and Measurement 56(4), 1265–1274 (2007)
6. Delsanto, S., Molinari, F., Liboni, W., Giustetto, P., Badalamenti, S., Suri, J.S.: User-independent plaque characterization and accurate IMT measurement of carotid artery wall using ultrasound. In: Proceedings of the 2006 IEEE Engineering in Medicine and Biology Society 28th Annual International Conference, vol. 1, pp. 2404–2407 (2006)
7. Destrempes, F., Meunier, J., Giroux, M.F., Soulez, G., Cloutier, G.: Segmentation in ultrasonic B-mode images of healthy carotid arteries using mixtures of Nakagami distributions and stochastic optimization. IEEE Transactions on Medical Imaging 28(2), 215–229 (2009)
8. Faita, F., Gemignani, V., Bianchini, E., Giannarelli, C., Ghiadoni, L., Demi, M.: Real-time measurement system for evaluation of the carotid intima-media thickness with a robust edge operator. Journal of Ultrasound in Medicine 27(9), 1353–1361 (2008)
9. Furberg, C.D., Byington, R.P., Craven, T.E.: Lessons learned from clinical trials with ultrasound end-points. Journal of Internal Medicine 236(5), 575–580 (1994)
10. Golemati, S., Stoitsis, J., Sifakis, E.G., Balkizas, T., Nikita, K.S.: Using the Hough transform to segment ultrasound images of longitudinal and transverse sections of the carotid artery. Ultrasound in Medicine and Biology 33(12), 1918–1932 (2007)
11. Liang, Q., Wendelhag, I., Wikstrand, J., Gustavsson, T.: A multiscale dynamic programming procedure for boundary detection in ultrasonic artery images. IEEE Transactions on Medical Imaging 19(2), 127–142 (2000)
12. Liguori, C., Paolillo, A., Pietrosanto, A.: An automatic measurement system for the evaluation of carotid intima-media thickness. IEEE Transactions on Instumentation and Measurement 50(6), 1684–1691 (2001)

13. Loizou, C.P., Pattichis, C.S., Pantziaris, M., Tyllis, T., Nicolaides, A.: Snakes based segmentation of the common carotid artery intima media. Medical and Biological Engineering and Computing 45(1), 35–49 (2007)
14. Molinari, F., Delsanto, S., Giustetto, P., Liboni, W., Badalamenti, S., Suri, J.S.: User-independent plaque segmentation and accurate intima-media thickness measurement of carotid artery wall using ultrasound. In: Advances in Diagnostic and Therapeutic Ultrasound Imaging, pp. 111–140. Artech House, Norwood (2008)
15. Molinari, F., Liboni, W., Giustetto, P., Badalamenti, S., Suri, J.S.: Automatic Computer-based Tracings (ACT) in longitudinal 2-D ultrasound images using different scanners. Journal of Mechanics in Medicine and Biology 9(4), 481–505 (2009)
16. Molinari, F., Zeng, G., Suri, J.S.: An Integrated Approach to Computer-Based Automated Tracing and IMT Measurement for Carotid Artery Longitudinal Ultrasound Images. In: Atherosclerosis Disease Management, pp. 221–251. Springer (2010)
17. Pignoli, P., Longo, T.: Evaluation of atherosclerosis with b-mode ultrasound imaging. The Journal of Nuclear Medicine and Allied Sciences 32(3), 166–173 (1988)
18. Schmidt, C., Wendelhag, I.: How can the variability in ultrasound measurement of intima-media thickness be reduced? studies of interobserver variability in carotid and femoral arteries. Clinical Physiology 19(1), 45–55 (1999)
19. Sivia, D.S., Skilling, J.: Data Analysis: A Bayesian Tutorial. Oxford University Press, USA (2006)
20. Stein, J.H., Korcarz, C.E., Mays, M.E., Douglas, P.S., Palta, M., Zhang, H., LeCaire, T., Paine, D., Gustafson, D., Fan, L.: A semiautomated ultrasound border detection program that facilitates clinical measurement of ultrasound carotid intima-media thickness. Journal of the American Society of Echocardiography 18(3), 244–251 (2005)
21. Stoitsis, J., Golemati, S., Kendros, S., Nikita, K.S.: Automated detection of the carotid artery wall in B-mode ultrasound images using active contours initialized by the Hough transform. In: Proceedings of the 2008 IEEE Engineering in Medicine and Biology Society 30th Annual International Conference 2008, pp. 3146–3149 (2008)
22. Touboul, P.J., Prati, P., Yves Scarabin, P., Adrai, V., Thibout, E., Ducimetiere, P.: Use of monitoring software to improve the measurement of carotid wall thickness by b-mode imaging. Journal of Hypertension 10(suppl. 5), S37–S42 (1992)
23. Wendelhag, I., Liang, Q., Gustavsson, T., Wikstrand, J.: A new automated computerized analyzing system simplifies readings and reduces the variability in ultrasound measurement of intima-media thickness. Stroke 28(11), 2195–2200 (1997)
24. Wendelhag, I., Wiklund, O., Wikstrand, J.: On quantifying plaque size and intima-media thickness in carotid and femoral arteries. comments on results from a prospective ultrasound study in patients with familial hypercholesterolemia. Arteriosclererosis, Thrombosis, and Vascular Biology 16(7), 843–850 (1996)
25. Williams, D.J., Shah, M.: A fast algorithm for active contours and curvature estimation. Computer Vision Graphics and Image Processing: Image Understanding 55(1), 14–26 (1992)
26. World Health Organization: Cardiovascular diseases. (March 2013), `http://www.who.int/mediacentre/factsheets/fs317/en/index.html`